

ACCEPTED

Facile synthesis of macroporous Ag and CuO monoliths as an efficient nonenzymatic electrochemical sensor and antimicrobial agent

Devendra Ahirwar¹, Mustri Bano¹, Imran Khan¹, Surendra Singh Gound², Mehraj Ud Din Sheikh¹, Rajesh Mondal², Farid Khan*¹

¹Nanomaterials Discovery Laboratory, Department of Chemistry,
Dr. Harisingh Gour University (A Central University), Sagar (M.P) 470003, India.

²Molecular Pathogenesis Laboratory, Department of Microbiology
Dr. Harisingh Gour University (A Central University), Sagar (M.P) 470003, India.

***Corresponding author:** - Prof. Farid Khan;

Nanomaterials Discovery Laboratory,

Department of chemistry,

Dr. Harisingh Gour University (A Central University), Sagar (M.P) 470003, India.

Email id: faridkhan58@yahoo.com

Phone: - +91-9425626334

Abstract

An efficient, green, acid free, reliable synthetic approach has been explored for the synthesis of macroporous silver and copper oxides monoliths. The concise tuning of macroporous materials using surfactants and structural directing agents like TiO₂ nanoparticles, and carbon nanotubes produces the monolith with a random network of pores, high porosity and surface area. The FESEM and BET analysis demonstrated the pore sizes of 40-500 nm and surface area in the range 40 to 114 m²/g. The XRD, EDAX and TGA analysis confirms the purity and crystallinity of monoliths. A comparative account of electrochemical sensing and antimicrobial applications has been developed. The electrochemical characterization reveals that Ag/TiO₂ and CuO/TiO₂ show excellent electrochemical properties and thus utilized as a nonenzymatic electrode material for simultaneous determination of Levodopa (L-dopa) and ascorbic acid (AA). The results show Ag/TiO₂/GCE show excellent sensing ability with a low detection limit as 0.034 μg mL⁻¹ and 0.014 μg mL⁻¹ in the concentration range of 0.1-20.0 μg mL⁻¹ and 0.01-2.0 μg mL⁻¹ for L-dopa and AA respectively. The synthesized monoliths have been tested for antimicrobial susceptibility against the eight gram-positive and gram-negative strains. The macroporous Ag/CNT exhibited better antimicrobial results against strains of *Klebsiellapneumoniae*, *Listeria monocytogenes*, *Vibriovulnificus* and *Bacillus subtilis*.

Keywords: Macroporous Ag; Macroporous CuO; Simultaneous electrochemical sensing; nonenzymatic electrode material; Antimicrobial activity;

1. Introduction

Metallic macroporous nanomaterials of silver (Ag) and copper oxide (CuO) monoliths are dynamic and highly efficient promising materials for diverse electrochemical and biomedical applications e.g. chemical sensing, energy devices, supercapacitors, and antimicrobial activity photocatalysis and widely used as heterogeneous catalysis environmentally benign [1-9]. Among the various noble metals and nanoporous-metal oxides i.e. Au and CuO have drawn attention due to its unique properties of conductivity, biocompatibility, chemical stability and mechanical flexibility [11]. The sensing and antimicrobial capability of Nanoporous materials have been generally evolved since last few years due to their high surface areas, external porosity and degree of crystallinity. Various techniques have been reported for the synthesis of porous Ag and CuO nanomaterials like electrochemical, sonochemical, solvothermal, microwave, photochemical, radiation assisted process [5-10, 12-16]. Although the development of reliable, green, economic and size controllable synthesis scheme of porous noble metal (micro-, meso- and macro-structured) nanomaterials is still a challenging task. The surface properties of nanoporous materials have been varied with varying porosity, pore size, composition and pore size distribution.

The present study is focused on the synthesis of macroporous Ag and CuO monoliths using Tween-80 as a reducing agent via a modified sol-gel route without using an acidic or basic medium i.e. “green synthesis approach”. The present synthesis protocol is controllable and does not use high temperature, pressure, and toxic chemicals. The titanium dioxide nanoparticles (TiO_2) and carbon nanotubes (CNTs) were used as structural directing agents to produces the monolith having high porosity and surface area with a three-dimensional random network of pores. The CNTs and TiO_2 help to increase the structural and physical properties like electrical conductivity, chemical stability, surface area [4, 17-20]. Although synthesized monolith has high surface/volume ratio, high mechanical strength and chemically variable morphologies.

The synthesized macroporous Ag and CuO and their monoliths (Ag/CNT, Ag/ TiO_2 , CuO/CNT and CuO/ TiO_2) were tested for their electrochemical and antimicrobial properties. The monoliths were used to fabricate the modified electrode and their sensing ability was investigated for the simultaneous determination of L-dopa and AA. The electrocatalytic behaviour was analysed using cyclic voltammetry (CV) and differential pulse voltammetry (DPV). L-dopa is a naturally producing dietary supplement and psychoactive drug. It is produced from the amino acids like L-phenylalanine and L-tyrosine in the brain and mammalian body. L-dopa is used as therapeutic drug in the treatment of Parkinson's disease and used by the brain to

generate dopamine which balanced the deficiency of dopamine in the organism and decreases the symptoms of Parkinson's disease [21-23]. AA is generally found in the extracellular fluid of the central nervous system and serum and plays a vital role in the metabolic reaction. It works as an antioxidant and essential nutrient for human being [24-25]. AA is recommended as effective preservative and antioxidant compound for food beverages. It has medicinal importance to increase high density lipoprotein formation, regulate cholesterol and triglyceride formation, lowers blood sugar and insulin [26].

Since the last decades, several reports show nanoparticles of Ag and Cu and their nanocomposite compounds are effective antimicrobial agents [2-6, 27-32]. The comparative bank of antibacterial effects of the synthesized Ag and CuO monoliths was created by analyzing them against eight group of bacterial isolates (gram negative and gram-positive bacteria) namely, *Escherichia coli* (MTCC 9537), *Salmonella enterica* (MTCC 734), *Staphylococcus aureus* (MTCC 1144), *Listeria monocytogenes* (MTCC 1143), *Klebsiella pneumoniae* (MTCC 109), *Clostridium sporogenes* (MTCC 1349), *Vibriovulnificus* (MTCC 1145) and *Bacillus subtilis* (MTCC 1272). Their activity can be enhanced by modification of surface morphology. Due to the growing bacterial resistance against diverse group of antibiotics, researchers from worldwide gained interest to look for newer antimicrobial agents. The metal nanoparticles may become the solution for development of microbial resistant compound.

2. Material and Chemicals

Tween-80 (molecular weight = 1310 Daltons, non-ionic surfactant), titanium dioxide nanoparticles (TiO_2 NPs with purity 99.5% and average particle size 21 nm), structure directing agents such as dextran (2×10^6 M) and carbon nanotubes (CNT) were purchased from Sigma Aldrich (St Louis, U.S.A.). Silver nitrate and Copper nitrate trihydrate were purchased from BDH (British drug house limited, England) and used as a precursor. All the experimental solutions were prepared using double distilled water.

3. Experimental

3.1 Synthesis of hierarchically macroporous silver monoliths

In a typical synthesis, 2.0 g of silver nitrate (50 wt %) in 2.0 g of double distilled water (50 wt %) was added to 2.0 g of soft template Tween-80 (14.81 wt %) in 11.50 g of double distilled (85.19 wt %) and stirred vigorously. A paste of dextran prepared by dissolving 1g dextran (33.33 wt %, $M_w = 2 \times 10^6$ Daltons) in 2 g distilled water (66.33 Wt %) was added to Ag/Tween-80. The resulting gel (Ag/Tween-80/dextran) was stirred at room temperature for 1 h

to form the paste which gradually became dark in colour. Similarly, Ag/CNT/Tween-80/dextran and Ag/TiO₂/Tween-80/dextran monoliths were prepared using the above protocol by adding 4.0 g dextran (57.14 wt %) in 3.0 g of ultrapure water (42.14 wt %), 0.10 g of single-wall carbon nano tubes (SWCNT) and 0.25 g of TiO₂ NPs separately to the Ag/Tween-80/dextran gel. The resulting gels were aged for 48 h at room temperature and then calcined at 400 °C for 2 h at a heating rate of 2 °C/min followed by cooling at a rate of 2 °C/min to room temperature in an Elite thermal system furnace. Finally, after calcination Ag/Tween-80/dextran, Ag/CNT/Tween-80/dextran and Ag/TiO₂/Tween-80/dextran was converted into macroporous Ag, Ag/CNT, and Ag/TiO₂ respectively.

3.2. Synthesis of hierarchically macro/mesostructured porous copper-oxide monoliths

Macroporous CuO monoliths were prepared by dissolving 2.0 g of copper(II) nitrate trihydrate in 2.0 g of double distilled (50 wt %) and 2.0 g of Tween-80 (14.81 wt %) in 11.5 g of double distilled (85.19 wt %) at 25 °C. A paste of dextran prepared by dissolving 1 g dextran (33.33 wt %, Mw = 2×10⁶ Daltons) in 2 g distilled water (66.33 wt %) was added to CuO/Tween-80. The gel was heated for 1 h at 55 °C on a magnetic stirrer to form a paste which gradually became light blue in colour. The resulting gel (CuO/Tween-80/dextran) was aged for 2-3 days at room temperature and then calcined at 400 °C for 2 h at a heating rate of 1 °C min⁻¹ followed by cooling at a rate of 1 °C min⁻¹ to room temperature in an Elite thermal system furnace. Similarly, CuO/CNT/Tween-80/dextran and CuO/TiO₂/Tween-80/dextran monoliths were prepared using the above protocol by adding 4.0 g dextran (57.14 wt%) in 3.0 g of ultrapure water (42.14 wt%), 0.10 g of single-wall carbon nanotubes (SWCNT) and 0.25 g of TiO₂ NPs separately to the CuO/Tween-80/dextran gel. The resulting gels were calcined at 400 °C with the same heating and cooling rate. Finally, after calcination CuO/Tween-80/dextran, CuO/CNT Tween-80/dextran, and CuO/TiO₂/Tween-80/dextran were converted into macroporous CuO, CuO/CNT, and CuO/TiO₂ respectively. The systematic pathway of synthesis of macroporous Silver and CuO showed in **Scheme 1**.

4. Structural characterization

The structural studies i.e. phase purity and composition of macroporous silver and copper monoliths were examined by using Bruker D-8 Advance powder X-ray diffractometer (PXRD) equipped with Cu K α ($\lambda = 1.5418 \text{ \AA}$) with scan rate 2° min⁻¹ (steps: 0.02°) and diffraction angle range 10-90°. The X-ray patterns obtained for macroporous Ag (**Fig. 1a**), Ag/CNT (**Fig. 1b**) and Ag/TiO₂ (**Fig. 1c**) showed reflection peaks at d spacings of 2.37, 2.06, 1.45, 1.23 and 1.18 Å,

which indexed to lattice planes as (111), (200), (220), (311), and (222) respectively (JCPDS No. 4.783). These lattice planes correspond to face centered cubic unit cell structures associated with $Fm\bar{3}m$ symmetry. The sharp and intense peaks in XRD patterns are evident for high crystallinity of the synthesized sample. In **Fig. 1c**, small noises like peaks of TiO_2 nanoparticles reveal that TiO_2 NPs are buried inside the macroporous Ag monolith. The PXRD patterns of macroporous CuO (**Fig. 1d**), CuO/CNT (**Fig. 1e**) and CuO/ TiO_2 (**Fig. 1f**) show clear resolved peaks with reflections at d spacings of 2.75, 2.52, 2.32, 1.86, 1.71, 1.58, 1.50, 1.41, 1.40, 1.30, 1.26, and 1.16 Å which correspond to lattice planes as (110), (002), (200), (-202), (020), (202), (-113), (022), (-311), (311), (004), and (312) represents base-centered monoclinic unit cell (tenorite) crystal (JCPDS no. 04.783). The sharp XRD pattern without impurity peaks reveals the formation of pure macroporous CuO nanomaterials. In the case of CuO/ TiO_2 monoliths (**Fig. 1f**), small noise like peaks of TiO_2 nanoparticles confirms the encapsulation of CuO monoliths.

The surface morphology of macroporous CuO, CuO/ TiO_2 , CuO/CNT, Ag, Ag/ TiO_2 , and Ag/CNT monoliths were examined by using NOVA NANOSEM 450 field emission scanning electron microscope (FESEM) equipped with energy dispersive X-ray spectroscopy (EDAX). The overview of FESEM images (**Fig. 2**) clearly depicted the random network of pores in macroporous Ag and CuO and their monoliths (**Fig. 2a and 2d**). The pores are distributed in the range of 40-500 nm in the porous monoliths. The addition of TiO_2 nanoparticles and CNT increases the pore size and surface area. The addition of dextran as a structural directing agent helps to increase the porosity of the material. The CNTs are tubular in nature with intertwined, twisted tubes with an average diameter of 5-10 nm, well mixed in Ag and CuO monoliths (**Fig. 2c and 2f**). The TiO_2 nanoparticles were distributed and stacked on surface of CuO and Ag macroporous materials (**Fig. 2b and 2e**). The **Fig. 2g, 2h and 2i** exhibited the EDAX analysis to ensure the presence of pure Ag monolith, and TiO_2 nanoparticles encapsulated CuO and Ag monoliths respectively.

The N_2 sorption isotherms of the as-synthesized macroporous monoliths were analyzed by using AutoSorb 1Q2 instrument (Quantachrome instrument Inc.). The Bruauer- Emmett-Teller (BET) surface area was determined by physisorption of N_2 at 77 K while Helium gas was used for degassing of samples. Among the series of as-synthesized monoliths, exhibits a sorption isotherm (**Fig. 3a and f**) of the IUPAC classification, featuring the macroporous characteristics of Ag and CuO materials. In the sorption isotherms when P/P_0 is above 0.8 or close to 1, the macroporous Ag (a), Ag/CNT (b), Ag/ TiO_2 (c), CuO (d), CuO/CNT (e) and CuO/ TiO_2 (f) show a rise in values (**Fig. 3 a-f**), revealing the existence of pores which is consistent agreement with FESEM results. The surface area and pore diameter of the as-prepared monoliths show a

dramatic increase with the variation of encapsulating materials. The pore size distributions of all samples were calculated by BJH method. The encapsulation of TiO₂ nanoparticles and CNT in Ag and CuO greatly increases such parameters, as shown in **Table 1**.

The thermal studies of as-synthesized monoliths was carried out in Perkin elmer thermal analyzer using an alumina reference crucible at a heating rate of 2 °C min⁻¹. The TGA curves (**Fig. 4**) of macroporous Ag and CuO revealed an initial weight loss of 8-15 % from room temperature to 150-175 °C due to the removal of moisture. Similarly, in Ag and CuO monoliths, a weight drop of 25-40 % was observed between 190-360 °C due to the decomposition of AgNO₃, Tween-80 and dextran and Cu(NO₃)₂.3H₂O in respective monoliths. Consecutively 13 %, 12 %, 12 %, 11 %, 18 %, and 21 % mass of macroporous Ag (**Fig. 4a**), Ag/CNT (**Fig. 4b**), Ag/TiO₂ (**Fig. 4c**), CuO (**Fig. 4d**), CuO/CNT (**Fig. 4e**) and CuO/TiO₂ (**Fig. 4f**) respectively were remains to observe.

5. Electrochemical analysis

The electrochemical analyses were performed in metrohm autolab B.V. PGSTAT128N controlled with software NOVA version 1.10.1.9. A three-electrode system was used namely, saturated calomel electrode (SCE) as reference electrode and platinum wire as a counter electrode and bare and modified glassy carbon electrode (GCE, a diameter of 3.0 mm) were served as working electrode, respectively. Prior to the analysis, analyte was purged with pure nitrogen for 150 s, while stirring the solution for removal of oxygen.

5.1. Fabrication of modified electrode

For the fabrication of modified electrode, namely, macroporous Ag/GCE, Ag/CNT/GCE, Ag/TiO₂/GCE, macroporous CuO/GCE, CuO/CNT/GCE, and CuO/TiO₂/GCE, the individual dispersion of all synthesized monoliths (Macroporous Ag, Ag/CNT and Ag/TiO₂, macroporous CuO, CuO/CNT, and CuO/TiO₂ monoliths) were prepared. For which 5 mg synthesized monoliths were the dispersed separately in 10 mL of ethanol by ultra-sonication. The 10 µL of dispersed mixture was cast over the polished GCE surface and the solvent was allowed to evaporate at room temperature. Prior to the electrode modification, electrode surface was polished with alumina powders (0.05 µm and 0.1 µm) and then cleaned by sonication in 0.1 M HCl for 10 minutes and dried at room temperature. The electrochemical activation of modified GCEs was performed by using cyclic potential sweeps in the range of -1.0 to +2.0 V in 0.1 M nitric acid solution at the scan rate of 50 mVs⁻¹ to obtain a steady voltammogram. After each

electrochemical measurements, the electrode surface was cleaned by rinsing it with distilled water and then cyclic sweeps in the reverse direction (1.0 V to 0.0 V) in phosphate buffer.

5.2. Electrochemical properties of Ag and CuO monoliths modified GCEs

The electrochemical properties of all Ag and CuO monoliths modified GCEs were evaluated by performing cyclic voltammetry using 1.0 mM $\text{K}_3\text{Fe}(\text{CN})_6$ probe with 0.1 M KCl solution at the scan rate of 50 mVs^{-1} (Fig. 5a). The well defined quasi-reversible peak was observed represents one electron redox behavior of $\text{Fe}(\text{CN})_6^{3-/4-}$ ions. The electrochemical surface area was calculated by recording cyclic voltammetric measurements at variable scan rates and by applying Randles-Sevcik equation [10]:

$$I_{pa} = 0.4463 \left(\frac{F^3}{RT} \right)^{1/2} n^{3/2} A_0 D_0^{1/2} C v^{1/2} \quad (1)$$

Where I_{pa} is anodic peak current, n is the number of electrons transferred, A_0 is surface area of the electrode (cm^2), D_0 is diffusion coefficient, C is concentration of $\text{Fe}(\text{CN})_6^{3-/4-}$ and v is the scan rate, R is molar gas constant ($8.314 \text{ JK}^{-1}\text{mol}^{-1}$) and F is Faraday's constant (96480 C mol^{-1}). For 1.0 mM $\text{K}_3\text{Fe}(\text{CN})_6$ in 0.1 M KCl at temperature, $T = 298 \text{ K}$, $n = 1$ and $D_0 = 7.6 \times 10^{-6} \text{ cm}^2\text{s}^{-1}$. The surface area was calculated from the slope obtained from the plot of I_{pa} versus $v^{1/2}$. In the present study, the surface area of the b-GCE was calculated as 0.0460 cm^2 and for macroporous Ag/GCE, macroporous CuO/GCE, Ag/CNT/GCE, CuO/CNT/GCE, Ag/TiO₂/GCE, and CuO/TiO₂/GCE found to be 0.157 cm^2 , 0.235 cm^2 , 0.437 cm^2 , 0.552 cm^2 , 0.812 cm^2 and 0.977 cm^2 respectively. The ΔE_p (anodic and cathodic peak separation) for b-GCE was calculated to be 0.541 V. After being modified with macroporous CuO and macroporous Ag, ΔE_p was decreased to 0.485 V and 0.445 V respectively. The peak current for $\text{Fe}(\text{CN})_6^{3-/4-}$ ions was also increased by 43 % and 64 % respectively. The subsequent modification of GCEs with CuO/CNT, Ag/CNT, CuO/TiO₂ and Ag/TiO₂ monoliths, decrease the value of ΔE_p as 0.384 V, 0.307 V, 0.238 V and 0.205 V respectively with increase in peak currents by 86 %, 98 %, 112 %, and 140 % respectively. The obtained values indicate the high conductivity of Ag/TiO₂/GCE and Cu/TiO₂/GCE with relatively high electrochemical surface area, favours the faster and easier charge transfer on the electrode surface.

5.3. Simultaneous voltammetric determination of L-dopa and Ascorbic acid

The electrocatalyzed nonenzymatic voltammetric behaviour of L-dopa and AA on bare and monoliths modified GCEs was investigated by recording cyclic voltammograms (CVs). The CV curves of $1.0 \times 10^{-6} \text{ M}$ AA in 0.02 M phosphate buffer solution (pH 7.0) show a well defined

irreversible, single anodic peak at 0.550 V during the potential sweep of -1.0 V to 1.0 V (**Fig. 5b**). This peak is attributed to the oxidation of AA, with no peak observed in the cathodic scan, indicating the irreversible nature of the oxidation process. Similarly 1.0×10^{-6} M L-dopa in 0.02 M phosphate buffer solution (pH 7.0) was analyzed with CV sweeps in the potential range of -1.6 V to 0.3 V (**Fig. 5c**). A well defined reversible peaks, anodic peak at -0.540 V, and the cathodic peak at -0.200 V were obtained, attributed to the complete redox behaviour of L-dopa. The significant higher peak intensity was observed at Ag/TiO₂/GCE, and CuO/TiO₂/GCE than macroporous Ag/GCE, macroporous CuO/GCE, Ag/CNT/GCE, CuO/CNT/GCE and b-GCE. This confirms the increased electrocatalytic behavior towards L-dopa and AA. The efficiency of electrodes for simultaneous analysis of L-dopa and AA were tested with CVs. The CV of 10.0×10^{-6} M L-dopa and 1.0×10^{-6} M AA in phosphate buffer (pH 7.0) was recorded at the scan rate of 50 mVs⁻¹ in the potential range of -1.0 V to 1.0 V (**Fig. 5d**). The concentration of AA influences peak generation of L-dopa, therefore 10 times higher concentration was taken for obtaining sharp and clear voltammogram. Ag/TiO₂/GCE and CuO/TiO₂/GCE show the enhanced peak intensity of these biomolecules analyte, possibly due to the increase in electron transfer rate, high electroactive surface area and excellent electrode conductivity. The quantification efficiency of Ag/TiO₂/GCE and CuO/TiO₂/GCE for simultaneous nonenzymatic voltammetric sensing of L-dopa and AA was evaluated by recording differential pulse voltammograms (DPVs) at the variable concentration in phosphate buffer (pH 7.0), as shown in **Fig. 6a and 6b**. The incorporated potential range of -1.0 V to 1.25 V at the scan rate of 50 mVs⁻¹. The best linear correlation was found in the concentration range of 0.1 – 20.0 µg mL⁻¹ for L-dopa and 0.01 – 2.0 µg mL⁻¹ for AA. The linear dependence of peak current intensity on the concentration of analyte was clearly depicted by linear regression equation and correlation coefficient (R²) expressed in **Table 2**. The analytical figures of merit for simultaneous determination i.e. limit of detection (LOD = 3 s/m, where *s* is the standard deviation of the intercept (n=5), *m* is the slope of the regression line [10]) and limit of quantification (LOQ = 10 s/m) are summarized in **Table 2**. The % RSD for five measurements at each concentration (n = 5) were ranged from 0.021 % to 0.148.

5.4. Stability, reproducibility, and repeatability

The repeatability of Ag/TiO₂/GCE and CuO/TiO₂/GCE was evaluated by analyzing peak currents of 20 successive DPV measurements in a mixture solution of 10.0×10^{-6} M L-dopa and 1.0×10^{-6} M AA in phosphate buffer (pH 7.0). The %RSD for L-dopa and AA were obtained to be 0.052 and 0.086 at Ag/TiO₂/GCE while 0.085 and 0.015 at CuO/TiO₂/GCE respectively indicate that electrode surface was not foul by the oxidation products. In order to analyze the

reproducibility, five Ag/TiO₂/GCE and CuO/TiO₂/GCE was prepared under the same conditions and used to record DP voltammogram of the same samples. The % RSD of peak current and peak potential obtained from the average of five replicated analysis are 0.310 % and 0.410 % for Ag/TiO₂/GCE respectively and 0.562 % and 0.382 % for CuO/TiO₂/GCE. The stability of Ag/TiO₂/GCE and CuO/TiO₂/GCE was investigated over a period of one month by storing them in 0.02 M phosphate buffer (pH 7.0). The current response of L-dopa and AA was decreased slightly by 2.1 % and 2.5 % respectively in first 18 days and after that sensor retained 94 % - 90 % of its initial peak response for remaining days. Therefore, the result manifests that the modified electrode exhibited good fabrication reproducibility, repeatability and stability which makes the best candidate to detect L-dopa, and AA concentration in the practical clinical analysis.

6. Antimicrobial activity

To evaluate the antibacterial activity of synthesized monoliths, eight pathogenic bacterial strains have been chosen e.g. *Escherichia coli* (MTCC 9537), *Salmonella enterica* (MTCC 734), *Staphylococcus aureus* (MTCC 1144), *Listeria monocytogenes* (MTCC 1143), *Klebsiellapneumoniae* (MTCC 109), *Clostridium sporogenes* (MTCC 1349), *Vibriovulnificus* (MTCC 1145), and *Bacillus subtilis* (MTCC 1272) obtained from microbial type culture collection (MTCC) from the Institute of microbial technology (IMTECH), Chandigarh, India. Muller-Hinton agar (MHA) medium (Himedia, Mumbai) was used for cultivation. The constituents of the media include-300 gms/liter beef infusion, 1.5 gms/liter soluble starch, 17.5 gms/liter casein acid hydrolysate, 17 gms/liter Agar-Agar and suspended in one liter of double distilled water, and pH 7.2 ±0.1. The antimicrobial activity of synthesized different macroporous monoliths (CuO, Cu/TiO₂, CuO/CNT, Ag, Ag/TiO₂ and Ag/CNT) dissolved (100 µg ml⁻¹) in double distilled sterile water was tested against above mentioned pathogens by Kirby-Baur disc diffusion for standard or as a control activity and used well diffusion method for macroporous materials described in CLSI guidelines-2017. Kanamycin disc (30mcg/disc) was used as a positive control. The diameter of the zone of inhibition was measured after incubation for overnight at 37 °C. Experiments were done in triplicates and repeated three times and the mean results are represented in **Table 3**. The best antibacterial results were obtained for *Klebsiellapneumoniae* (MTCC 109), *Listeria monocytogenes* (MTCC 1143), *Vibriovulnificus* (MTCC 1145) and *Bacillus subtilis* (MTCC 1272) out of 8 pathogens, as shown in **Fig. 7**. The **Fig. 8** showed the graphical representation of growth inhibition at wells loaded with 100 µg mL⁻¹ concentrations of macroporous Ag and CuO

monoliths as compared to positive control Kanamycin disc (30 mcg/disc). Their activity can be enhanced by concise tuning of surface area and surface morphology. In this comparative study, the results show that macroporous Ag combined with CNT exhibited better antimicrobial susceptibility against the gram-positive and gram-negative strains tested. In case of macroporous CuO, higher concentrations were required to achieve high antibacterial activity. However, macroporous Ag and CuO are small enough to disrupt bacterial cell membranes and gain entry in order to disrupt enzyme function. Likewise, these monoliths have been shown to attach to the bacterial cell surface and penetrate inside, where intracellular targets, including respiratory enzymes, are disrupted.

6.1. Mechanisms of antibacterial effects of macroporous silver materials

In the literature, there are various theories and mechanisms for antimicrobial action of silver and copper nanomaterials. The macroporous Ag/CNT releases the Ag^+ ions, which interacts with the bacterial cell membrane to causes chemical and structural changes. The permeation of cell membrane and disrupts of the cell wall causes cell death. In another bactericidal mechanism, the released Ag^+ ions and Ag/CNT gets accumulated and aggregated near the cell wall, consequently forms free radicals and reactive oxygen which have the ability to break the cell membrane and leads to cell death [28-29]. The plausible mechanism of antibacterial activity of Ag/CNT monolith is illustrated in **Fig. 9**. The similar mechanism also occurs with macroporous CuO monoliths [30]. The Ag^+ and Cu^{2+} ions generate active free radicals and reactive oxygen that are responsible for damaging the bacterial cells. The Ag^+ and Cu^{2+} ions also have the ability to interact with the thiol (-SH) group of DNA, proteins, and enzymes and prevented the DNA replication leading to enhanced pyrimidine dimerization. The highly stable interaction of ions with soft bases of DNA damages the bacterial cell [4]. In CNT supported macroporous materials, CNT provides the physical surface to Ag and Cu ions for interaction with the cell membrane [40-41]. The surface area, the pore volume of Ag and strong metal-carbon adhesion with CNT make a significant factor for their antibacterial property.

The present study evaluated the antimicrobial behaviour of porous Ag and CuO monoliths by encapsulations of CNT and TiO_2 . The antibacterial results reveal that Ag/CNT and CuO/CNT showed better activity than Ag/ TiO_2 and CuO/ TiO_2 despite high surface area materials, because of needle-like structural morphology of CNT attached. The CNTs penetrate the bacterial cell membrane and finally burst the cell. Here parallel and synergistic effect of CNTs works with CuO and Ag for exhibiting better antibacterial activity. However in case of TiO_2 NPs encapsulated with Ag and CuO which have spherical in shape, stacked and trapped in

the monoliths do not perform such antibacterial activity as free CNTs encapsulating monolith did. [31-35]. In terms of the antimicrobial property of CNTs, the tendency to translocate cellular barriers i.e. plasma membrane and nano-needle piercing of pathogen cell, by phenomenon is great considerable properties described [34, 35]. Numerous laboratories use various types of CNTs based nano-materials have now reported their cellular uptake by a wide range of cells [34, 36–39]. This study solves the problem of wastage of costly nanomaterials and helps to reduce the amount of antimicrobial agent with encapsulating the high cost TiO₂ NPs and CNTs in CuO and Ag monoliths such as TiO₂ NPs and CNTs by encapsulating porous monolith with the lesser amount.

Conclusion

An efficient, green, acid-free, reliable synthetic approach for fabrication of macroporous Ag and CuO monoliths have been explored. The procedure has a higher ability for concise tuning of macroporous materials by using different surfactants and structural directing agents. The synthesized monoliths were crystalline containing random network of pores which increases their porosity and surface area. The comparative study of electrochemical sensing and the antimicrobial study show the macroporous Ag/TiO₂ and CuO/TiO₂ monoliths show excellent electrochemical properties. The fabricated monoliths modified electrodes were efficaciously applied for nonenzymatic simultaneous determination of L-dopa and AA. The results show Ag/TiO₂/GCE show excellent sensing ability in comparison to other monolith modified electrode. It reports selective recognition, sensitive and precise determination with low detection limit. The as-synthesized macroporous Ag and CuO monoliths have found to be important antimicrobial agents. Their activity can be enhanced by concise tuning of surface morphology. However, macroporous Ag/CNT exhibited better the antimicrobial susceptibility against the gram-positive and gram-negative bacterial strains tested. The development of the non-toxic, eco-friendly and non-enzymatic bio molecule sensing material and antimicrobial agents such as macroporous metals and metal oxides will serve as an alternative to emergent sensing devices and traditional antibiotics, might be promising for future of medicine, pharmaceuticals and clinical analysis.

Acknowledgement

The authors acknowledge Department of Science & Technology, New Delhi for financial support, Sophisticated Instrumentation Centre and Department of Chemistry, Dr. Harisingh Gour Vishwavidyalaya (A Central University) Sagar, India for providing instrumentation facility.

Ethical Approval was not required.

There is no conflict of interest to all authors in this research article.

The International Standard Randomized Controlled Trial Number (ISRCTN) or ClinicalTrials.gov registration number is "Not applicable".

References

- [1] F.Q. Sun, W.P. Cai, Y. Li, L.C. Jia, F. Lu, Direct Growth of Mono- and multilayer nanostructured porous films on curved surfaces and their application as gas sensor, *Adv. Mater.* 17 (2005) 2872–2877.
- [2] I. Sondi, B. Salopek-Sondi, Silver nanoparticles as antimicrobial agent: a case study on *E.colias* a model for Gram-negative bacteria, *J. Colloid Interface Sci.* 275 (2004) 177–182.
- [3] G.A. Martínez-Castañón, N. Niño-Martínez, F. Martínez-Gutierrez, J.R. Martínez-Mendoza, F.Ruiz, Synthesis and antibacterial activity of silver nanoparticles with different sizes. *J. Nanopart Res* 10 (2008) 1343–1348.
- [4] G.A.Naikoo, M. Thomas, M.A. Ganaie, M.U.D. Sheikh, M. Bano, I.U. Hassan, F. Khan, Hierarchically macroporous silver monoliths using Pluronic F127: Facile synthesis, characterization and its application as an efficient biomaterial for pathogens, *J. Saudi Chem. Soc.* 20 (2016) 237–244.
- [5] Y. Cao, J. Fan, L. Bai, P. Hu, G. Yang, F. Yuan, Y. Chen, Formation of cubic Cu mesocrystals by a solvothermal reaction, *Cryst Eng Commun* 12 (2010) 3894–3899.
- [6] A. Melaiye, Z. Sun, K. Hindi, A. Milsted, D. Ely, D.H. Reneker, C.A. Tessier, W.J. Youngs, Silver (I)-imidazole cyclophane gem-diol complexes encapsulated by electrospun tectophilic nanofibers: formation of nanosilver particles and antimicrobial activity, *J. Am. Chem. Soc.* 127 (2005) 2285–2291.
- [7] T. Chang, Z. Li, G. Yun, Y. Jia, H. Yang, Enhanced Photocatalytic Activity of ZnO/CuO Nanocomposites Synthesized by Hydrothermal Method, *Nano-Micro Lett.* 5 (2013) 163–168

- [8] M. Jung, J. Scott, Y. H. Ng, Y. Jiang, R. Amal, CuO_x dispersion and reducibility on TiO₂ and its impact on photocatalytic hydrogen evolution, *Int. J. Hydrog. Energy* 39 (2014) 12499–12506.
- [9] S. Ko, J.I. Lee, H.S. Yang, S. Park, U. Jeong, Mesoporous CuO Particles Threaded with CNTs for High-Performance Lithium-Ion Battery Anodes, *Adv. Mater.* 24 (2012) 4451–4456.
- [10] I. Khan, U.J. Pandit, S.N. Limaye, Design of electrochemically modified fMWCNT-pencil graphite electrode decorated with Cu and Ag nanofilm and its electrocatalytic behavior towards Imazethapyr, *Electroanalysis* 29 (2017) 2423–2436.
- [11] J.J.L. West, N.J. Halas, Engineered nanomaterials for biphotonics applications: Improving sensing, imaging and therapeutics, *Annu. Rev. Biomed. Eng.* 5 (2003) 285–292.
- [12] L. Rodriguez-Sanchez, M.C. Blanco, M.A. Lopez-Quintela, Electrochemical synthesis of silver nanoparticles, *J Phys Chem B* 104 (2000) 9683–9688.
- [13] I. Perelshtein, G. Applerot, N. Perkas, G. Guibert, S. Mikhailov, A. Gedanken, Sonochemical coating of silver nanoparticles on textile fabrics (nylon, polyester and cotton) and their antibacterial activity, *Nanotechnology* 19 (2008) 245705–245711.
- [14] K. Shameli, M.B. Ahmad, W.M.Z.W. Yunus, N.A. Ibrahim, Y. Gharayebi, S. Sedaghat, Synthesis of silver/montmorillonite nano composite using-irradiation, *Int J Nanomed* 5 (2010) 1067–1077.
- [15] H. Yin, T. Yamamoto, Y. Wada, S. Yanagida, Large-scale and size-controlled synthesis of silver nanoparticles under microwave irradiation, *Mater Chem Phys* 83 (2004) 66–70.
- [16] K. Mallick, M.J. Witcomb, M.S. Scurrill, Polymer stabilized silver nanoparticles: A photochemicalsynis route, *J Mater Sci* 39 (2004) 4459–4463.
- [17] A. Merkoci, M. Pumera, X. Llopi, B. Perez, M. del Valle, S. Alegret, New materials for electrochemical sensing VI: Carbon nanotubes, *Trends Anal. Chem.* 24 (2005) 826–838.

- [18] X.H. Kang, Z.B. Mai, X.Y. Zou, P.X. Cai, J.Y. Mo, A sensitive nonenzymatic glucose sensor in alkaline media with a copper nanocluster/multiwall carbon nanotube-modified glassy carbon electrode, *Anal. Biochem.* 363 (2007) 143–150.
- [19] J.H. Lin, C.Y. He, Y. Zhao, S.S. Zhang, One-step synthesis of silver nanoparticles/carbon nanotubes/chitosan film and its application in glucose biosensor, *Sens. Actuators B* 137 (2009) 768–773.
- [20] L.C. Jiang, W.D. Zhang, Electrodeposition of TiO₂ nanoparticles on multiwalled carbon nanotube arrays for hydrogen peroxide sensing, *Electroanalysis* 21 (2009) 988–993.
- [21] P. Damier, E.C. Hirsch, Y. Agid, A.M. Graybiel, The substantia nigra of the human brain: II. Patterns of loss of dopamine-containing neurons in Parkinson's disease, *Brain* 122 (1999) 1437–1448.
- [22] A. Babaei, M. Sohrabi, A.R. Taheri, Highly sensitive simultaneous determination of L-dopa and paracetamol using a glassy carbon electrode modified with a composite of nickel hydroxide nanoparticles/multi-walled carbon nanotubes, *J. Electroanal. Chem.* 698 (2013) 45–51.
- [23] H.H. Takeda, T.A. Silva, B.C. Janegitz, F.C. Vicentini, L.H.C. Mattoso, O. Fatibello-Filho, Electrochemical sensing of L-dopa or carbidopa using a glassy carbon electrode modified with carbon nanotubes within a poly(allylamine hydrochloride) film, *Anal. Methods*, 8 (2016) 1274–1280.
- [24] U. Yogeswaran, S. Thiagarajan, S.M. Chen, Nanocomposite of functional multiwall carbon nanotubes with nafion, nano platinum, and nano biosensing film for simultaneous determination of AA epinephrine, and uric acid, *Anal. Biochem.* 1 (2007) 122–131.
- [25] S.J. Padayatty, A. Katz, Y.H. Wang, P. Eck, O. Kwon, J.H. Lee, S.L. Chen, C. Corpe, A. Dutta, S.K. Dutta, M. Levine, Vitamin C as an antioxidant: evaluation of its role in disease prevention, *J. Am. Coll. Nutr.* 1 (2003) 18–35.

- [26] A. Bossi, S.A. Piletsky, E.V. Piletska, P.G. Righetti, A.P.F. Turner, An assay for ascorbic acid based on polyaniline-coated microplates, *Anal. Chem.* 72 (2000) 4296–4300.
- [27] V. Thomas, M.M. Yallapu, B. Sreedhar, S.K. Bajpai, A versatile strategy to fabricate hydrogel–silver nanocomposites and investigation of their antimicrobial activity, *J. Colloid Interface Sci.* 315 (2007) 389–395S.
- [28] K. Cho, J. Park, T. Osaka, S. Park, The study of antimicrobial activity and preservative effects of nano silver ingredient, *Electrochim Acta* 51 (2005) 956–960.
- [29] S Hartsel, J. Bolard, Amphotericin B: New life for an old drug *Trends, Pharmacol Sci* 17 (1996) 445–449.
- [30] I. Perelshtein, G. Applerot, N. Perkas, G. Guibert, S. Mikhailov, A. Gedanken, Sonochemical coating of silver nanoparticles on textile fabrics (nylon, polyester and cotton) and their antibacterial activity, *Nanotechnology*, 19 (2008) 245705–245711.
- [31] A. E. Simon-Deckers, S. Loo, M. M. L’Hermite, N. Herlin-Boime, N. Menguy, C. E. Reynaud, B. Gouget, and M. Carrie`re, Size-, Composition- and Shape-Dependent Toxicological Impact of Metal Oxide Nanoparticles and Carbon Nanotubes toward Bacteria, *Environ. Sci. Technol.* 43 (2009) 8423–8429.
- [32] S. Kang, M. Herzberg, D. F. Rodrigues, and M. Elimelech, Antibacterial effects of carbon nanotubes: size does matter, *Langmuir*, 24 (2008) 6409–6413.
- [33] S. Kang, M. S. Mauter, M. Elimelech, Physicochemical determinants of multiwalled carbon nanotube bacterial cytotoxicity, *Environ. Sci. Technol.*, 42 (2008) 7528–7534.
- [34] K. Kostarelos, L. Lacerda, G. Pastorin, W. Wu, S. Wieckowski, J. Luangsivilay, S. Godefroy, D. Pantarotto, J.P. Briand, S. Muller, M. Prato, A. Bianco, Cellular uptake of functionalized carbon nanotubes is independent of functional group and cell type, *Nat Nanotechnol*, 2 (2007) 108–113.
- [35] L. Lacerda, S. Raffa, M. Prato, A. Bianco, K. Kostarelos, Cell-penetrating CNTs for delivery of therapeutics. *Nano Today*, 2 (2007) 38–43.

- [36] M. L. Becker, J. A. Fagan, N. D. Gallant, B. J. Bauer, V. Bajpai, E. K. Hobbie, S. H. Lacerda, K. B. Migler, J. P. Jakupciak, Length-dependent uptake of DNA-wrapped single-walled carbon nanotubes, *Adv Mater*, 19 (2007) 939-945.
- [37] N. W. Kam, Z. Liu, H. Dai, Carbon nanotubes as intracellular transporters for proteins and DNA: an investigation of the uptake mechanism and pathway, *Angew Chem Int Ed Engl* 45 (2006) 577–581.
- [38] Kang B, D. C. Yu, S. Q. Chang, D. Chen, Y. D. Dai, Y. T. Ding, Intracellular uptake, trafficking and subcellular distribution of folate conjugated single walled carbon nanotubes within living cells, *Nanotechnology*, 19 (2008) 375103–375111.
- [39] N.W. Shi Kam, T.C. Jessop, P. A.Wender, H. Dai, Nanotube molecular transporters: internalization of carbon nanotube-protein conjugates into Mammalian cells, *J Am Chem Soc* 1, 26 (2004) 6850–6851.
- [40] K. Kim, W. Jun, S. Sung, S. K. Moon, J. S. Choi, J.G. Kim, D.G. Lee, Antifungal effect of silver nanoparticles on dermatophytes microbial, *Biotechnol*, 18 (2008) 1482–1484.
- [41] E. Falletta, M. Bonini, E. Fratini, A.L. Nostro, G. Pesavento, A. Becheri, Clusters of poly (acrylates) and silver nanoparticles: structure and applications for antimicrobial fabrics *J. Phys. Chem. C*, 112 (2008) 11758–11766.

Table 1: N₂ adsorption-desorption results (surface area, pore volume and average pore diameter) of macroporous (1) Ag, (2) Ag/CNT, (3) Ag/TiO₂, (4) CuO, (5) CuO/CNT, and (6) CuO/TiO₂.

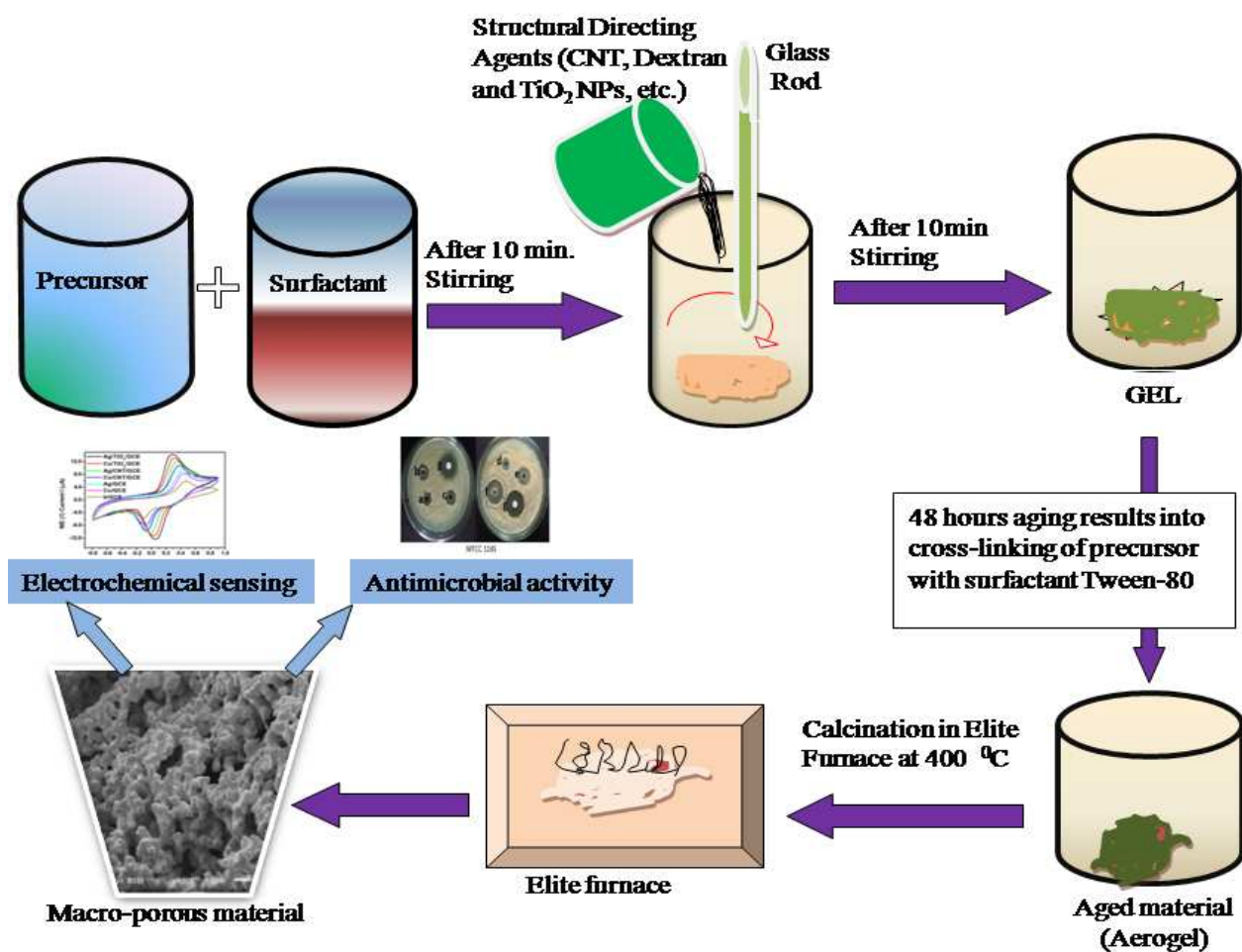
S. No.	Sample	BET surface area (m ² g ⁻¹)	Average pore diameter (nm)
1	Ag	40.175	46
2	Ag/CNT	42.442	56
3	Ag/TiO ₂	51.531	70
4	CuO	62.178	62
5	CuO/CNT	100.706	95
6	CuO/TiO ₂	114.068	100

Table 2: Analytical figure of merits for simultaneous voltammetric sensing of L-dopa and AA using differential pulse voltammetry.

Analyte	Electrode	Linear range (μg mL ⁻¹)	Linear regression equation	LOD (μg mL ⁻¹)	LOQ (μg mL ⁻¹)	Mean % RSD
L-dopa	Ag/TiO ₂ /GCE	0.01 - 2.0	Ip (μA) = 5.4843 (μg mL ⁻¹) LD + 2.9810; R ² = 0.988	0.034	0.114	0.021
	CuO/TiO ₂ /GCE		Ip (μA) = 4.2665 (μg mL ⁻¹) LD + 2.7503; R ² = 0.980	0.061	0.203	0.131
AA	Ag/TiO ₂ /GCE	0.1- 20.0	Ip (μA) = 7.1053 (μg mL ⁻¹) AA + 8.9031; R ² = 0.985	0.014	0.048	0.060
	CuO/TiO ₂ /GCE		Ip (μA) = 5.5003 (μg mL ⁻¹) AA + 7.73563, R = 0.985	0.030	0.102	0.148

Table 3: The zone of inhibition (mm) from wells loaded with $100 \mu\text{g mL}^{-1}$ a = CuO; b = Cu/TiO₂; c = CuO/CNT; d = Ag; e = Ag/TiO₂; f = Ag/CNT and K 30 = Kanamycin disc (30 mcg/disc).

Zone of inhibition (mm)								
S. No.	Pathogen	a	b	c	d	e	f	K30
1	MTCC 109	10	12	16	14	12	19	18
2	MTCC 734	12	14	19	14	14	18	20
3	MTCC 1143	13	15	20	12	14	20	21
4	MTCC 1144	13	15	20	14	12	19	19
5	MTCC 1145	12	14	18	13	15	21	23
6	MTCC 1272	10	12	16	12	16	22	23
7	MTCC 1349	12	13	17	13	18	20	19
8	MTCC 9537	12	14	14	13	16	16	18



Scheme 1. A schematic protocol for the synthesis of macroporous monoliths.

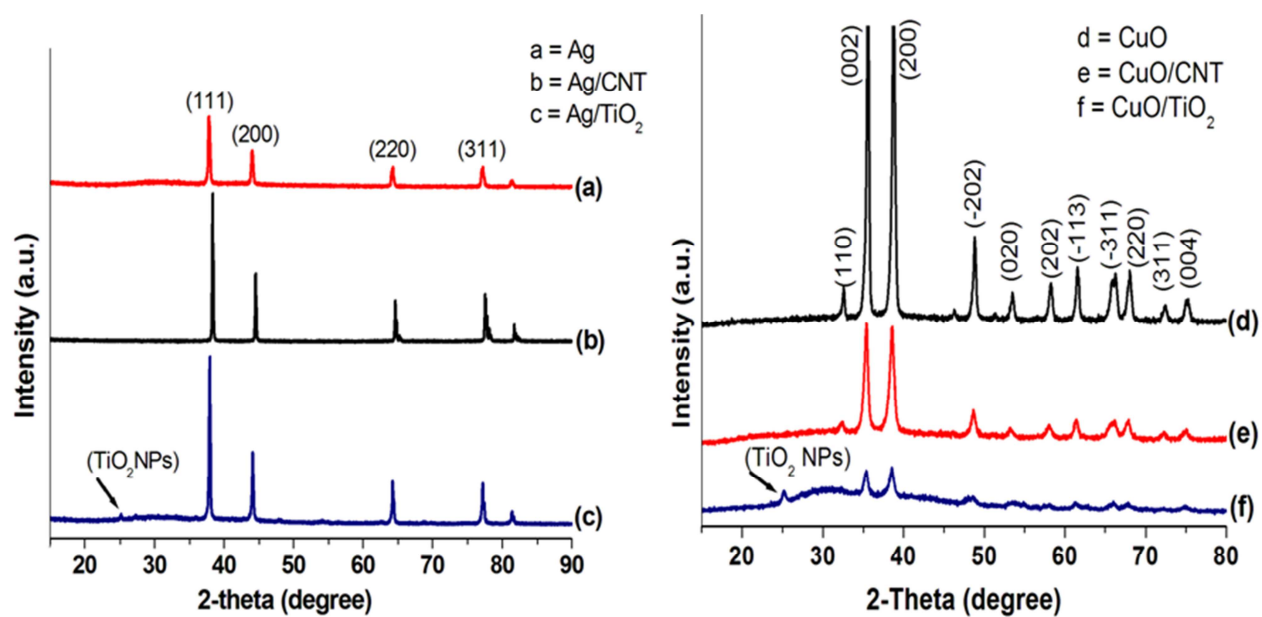


Fig. 1 P-XRD patterns of macroporous (a) Ag, (b) Ag/CNT, (c) Ag/TiO₂, (d) CuO, (e) CuO/CNT and (f) CuO/TiO₂.

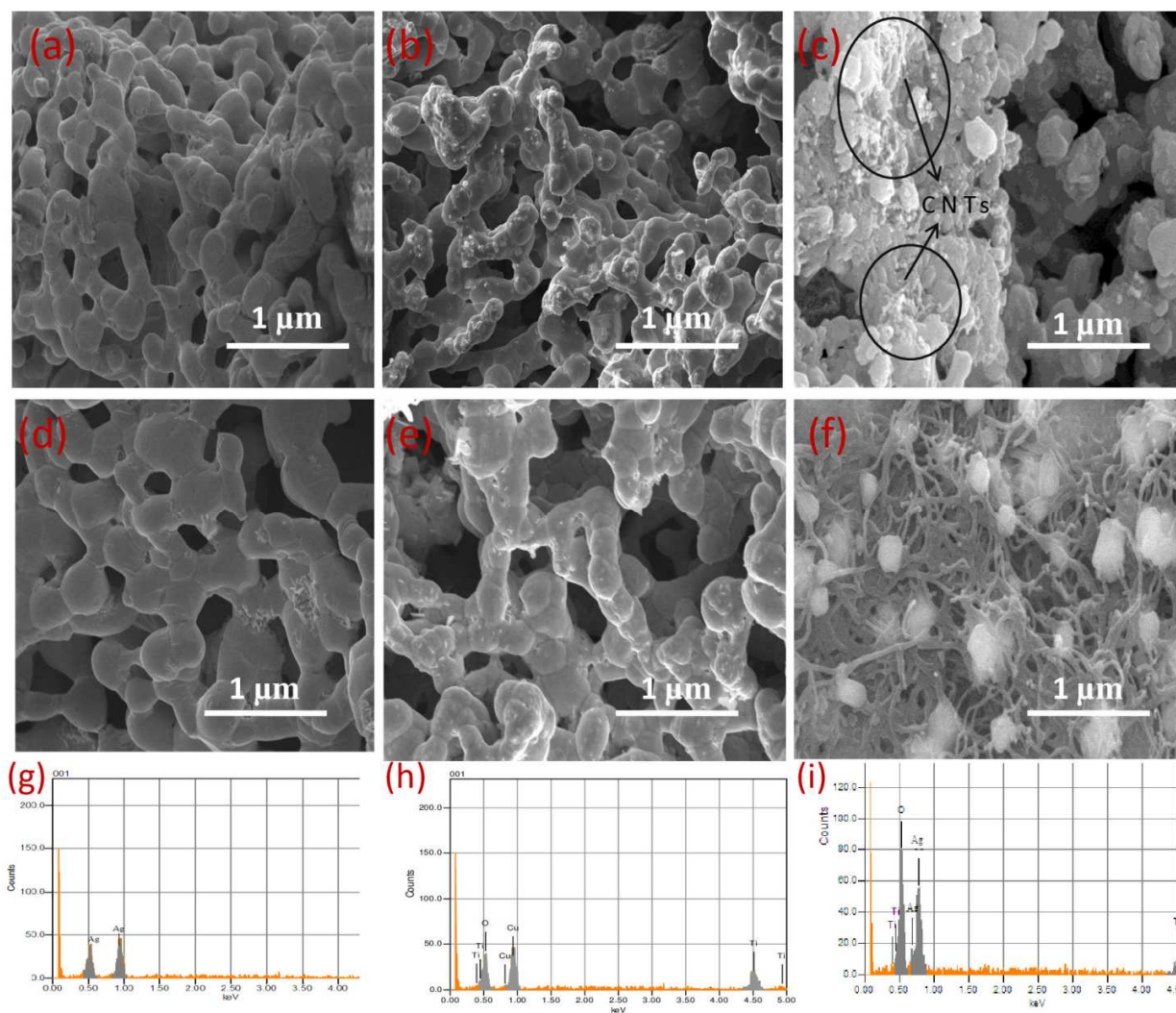


Fig. 2 SEM micrograph of (a) CuO, (b) CuO/TiO₂, (c) CuO/CNT, the black coloured circle showing the morphology of CNTs encapsulated in CuO (d) Ag, (e) Ag/TiO₂ and (f) Ag/CNT; EDAX analysis of (g) Ag, (h) CuO/TiO₂ and (i) Ag/TiO₂ monolith.

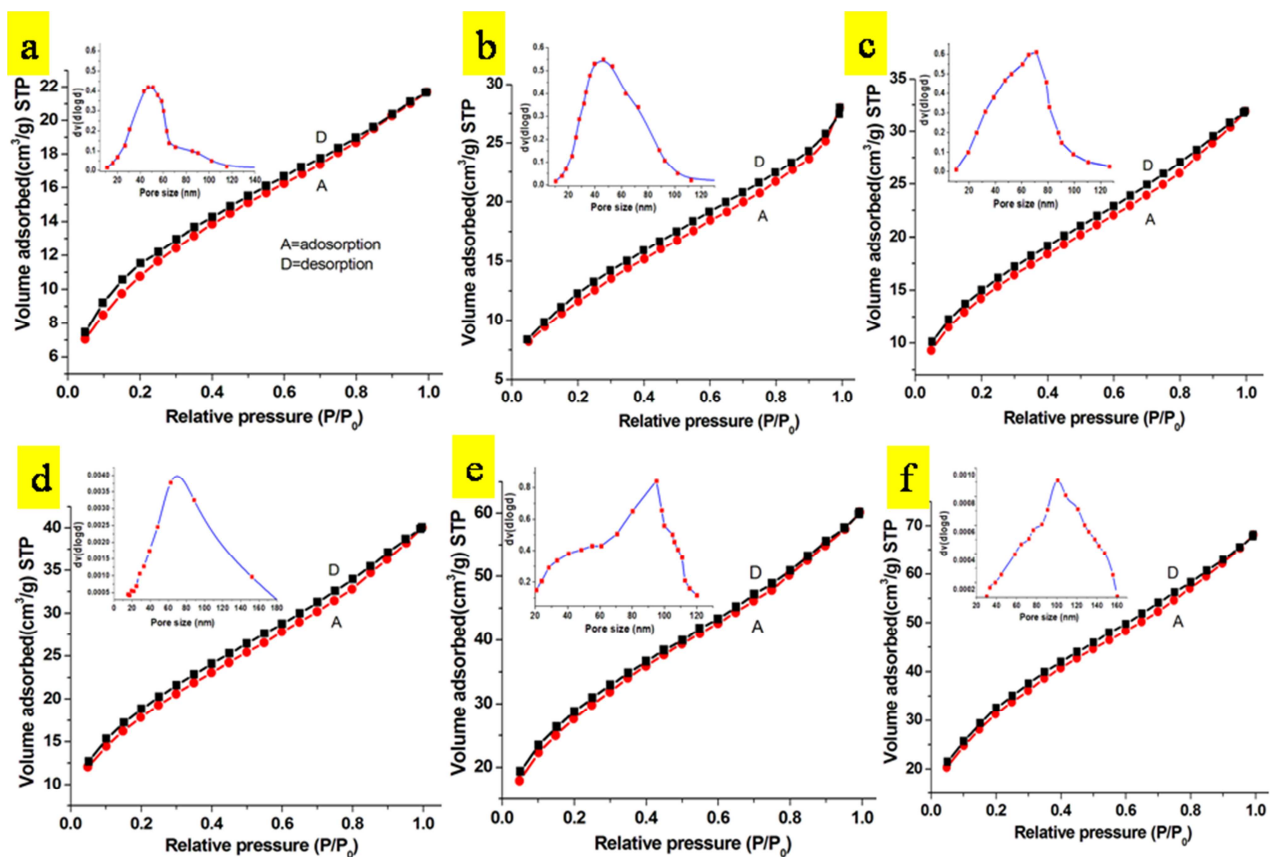


Fig. 3 N₂ adsorption-desorption isotherm of macroporous (a) Ag, (b) Ag/CNT, (c) Ag/TiO₂, (d) CuO, (e) CuO/CNT and (f) CuO/TiO₂, where A and D represents adsorption and desorption curves respectively.

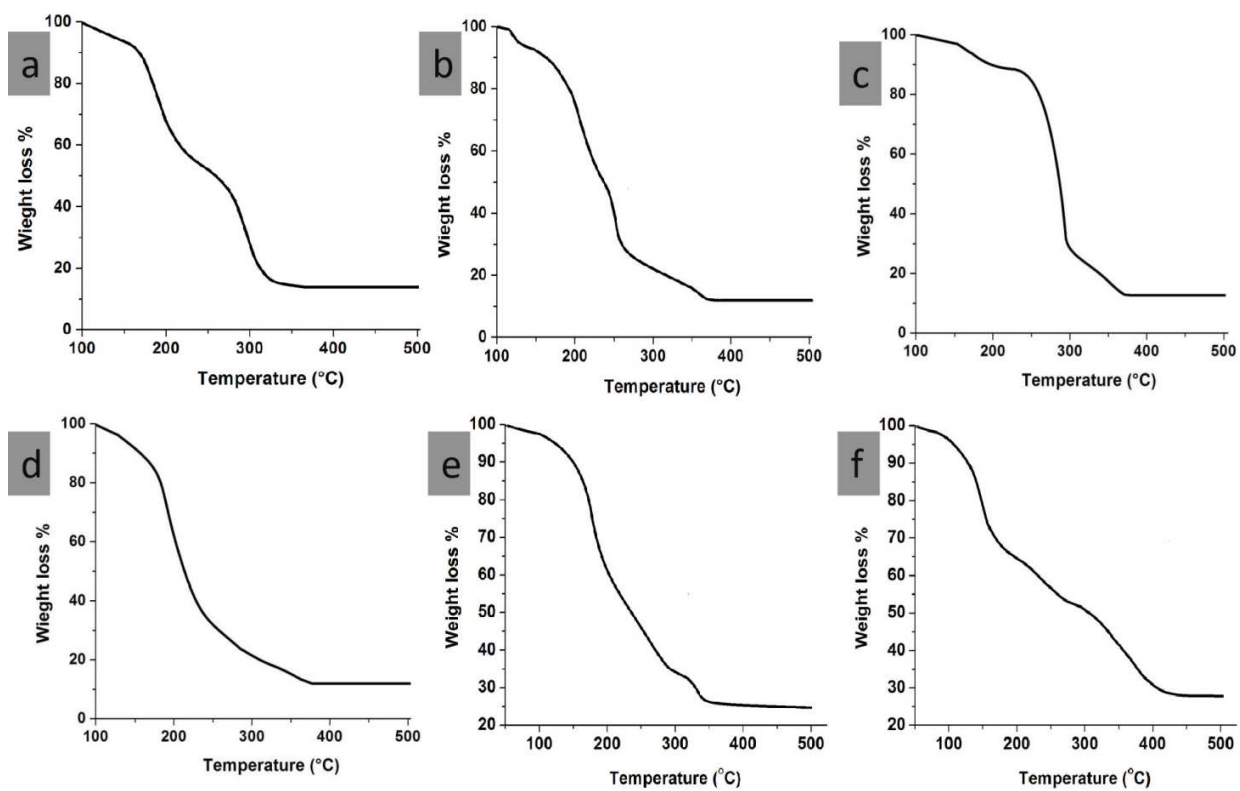


Fig. 4 TGA of macroporous (a) Ag, (b) Ag/CNT, (c) Ag/TiO₂, (d) CuO, (e) CuO/CNT and (f) CuO/TiO₂ before calculations.

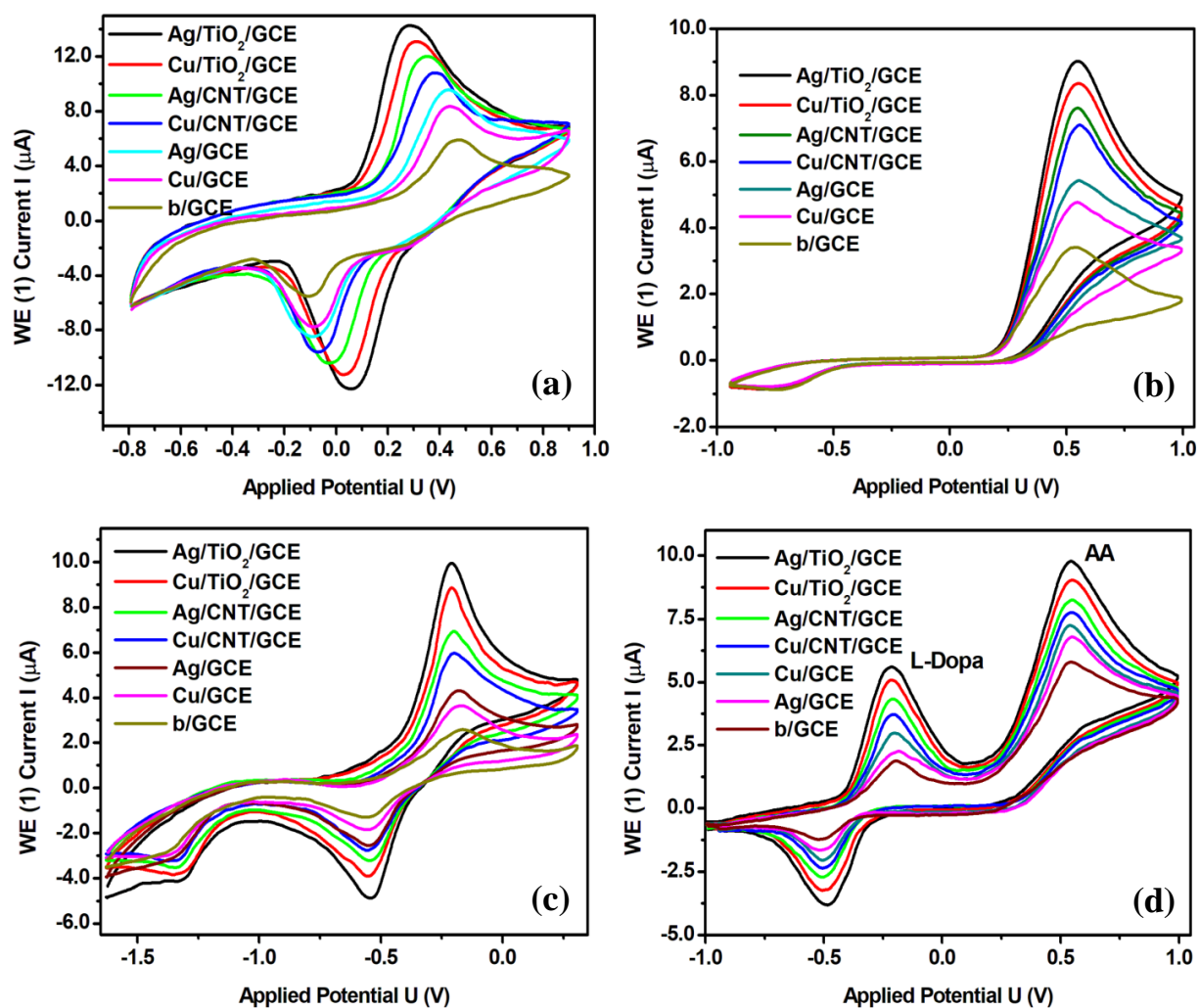


Fig. 5 (a-d) CV of (a) 1.0 mM Fe(CN)₆^{3-/4-} in 0.1 M KCl (b) 1.0 × 10⁻⁶ M Ascorbic acid, (c) 1.0 × 10⁻⁶ M Levodopa and (d) 10.0 × 10⁻⁶ M Levodopa and 1.0 × 10⁻⁶ M Ascorbic acid in phosphate buffer (pH 7) at bare and monoliths modified GCEs.

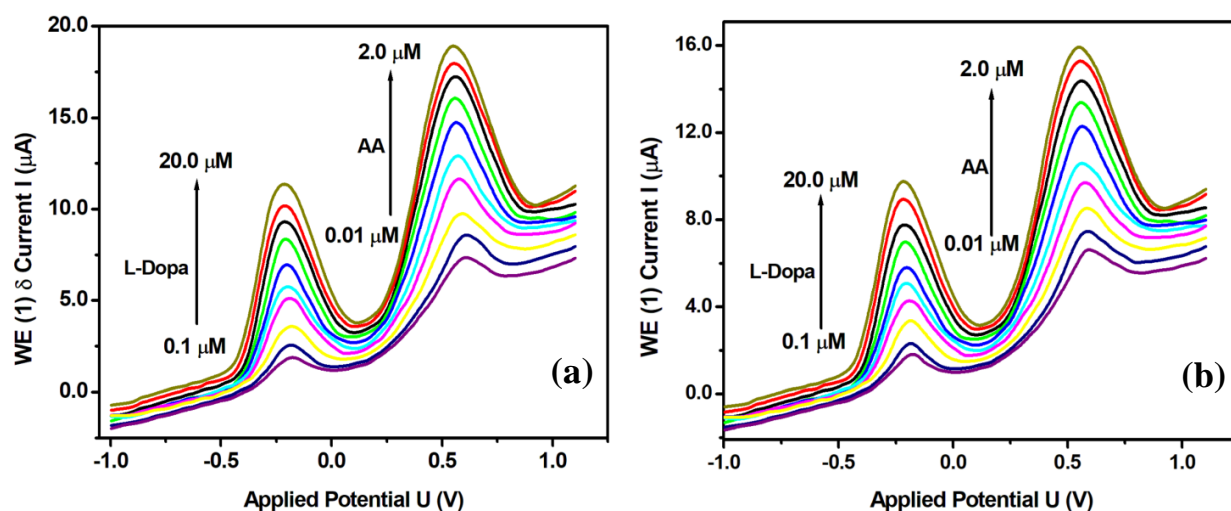


Fig. 6 DPV of simultaneous addition of different concentration of Ascorbic acid (0.01, 0.05, 0.1, 0.2, 0.4, 0.6, 0.8, 1.0, 1.5 and 2.0) $\mu\text{g mL}^{-1}$ and Levodopa (0.1, 0.5, 1.0, 2.0, 4.0, 6.0, 8.0, 10.0, 15.0 and 20.0) $\mu\text{g mL}^{-1}$ on (a) $\text{Ag/TiO}_2/\text{GCE}$ and (b) $\text{CuO/TiO}_2/\text{GCE}$.

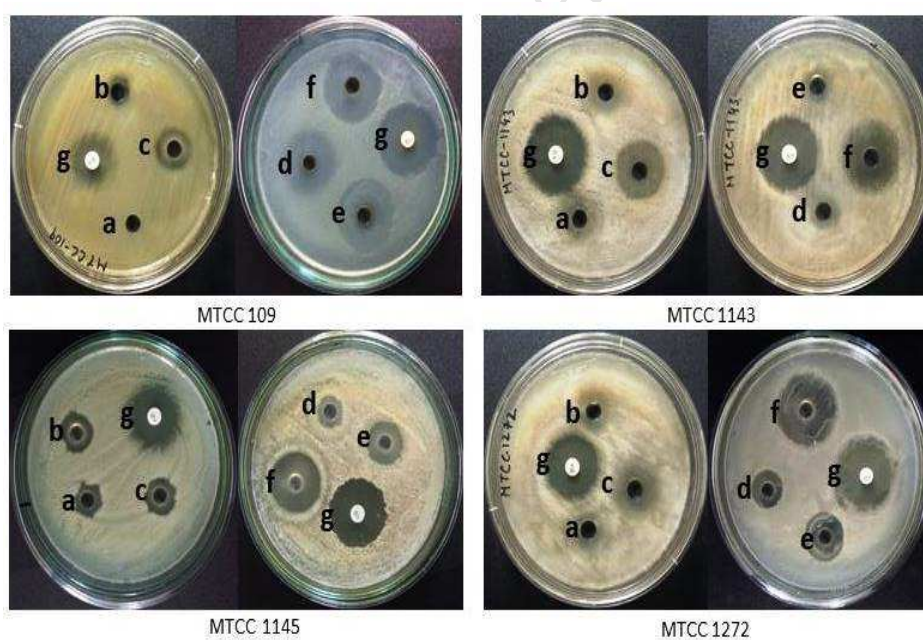


Fig. 7 Shows representative images of plates *Klebsiella pneumoniae* (MTCC 109), *Listeria monocytogenes* (MTCC 1143), *Vibrio vulnificus* (MTCC 1145) and *Bacillus subtilis* (MTCC 1272) and the zone of inhibition (mm) from wells loaded with $100 \mu\text{g mL}^{-1}$ a = CuO; b = Cu/TiO₂; c = CuO/CNT; d = Ag; e = Ag/TiO₂; f = Ag/CNT and g = Kanamycin disc (30 mcg/disc).

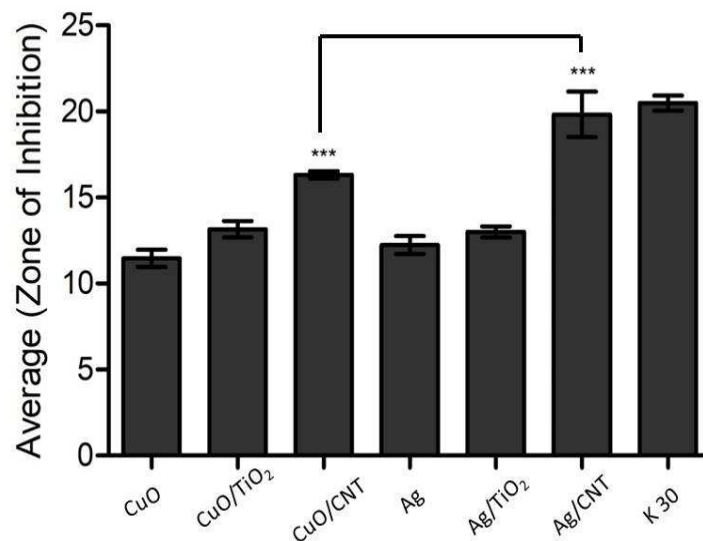


Fig. 8 The average zone of inhibition from wells loaded with $100 \mu\text{g ml}^{-1}$ of CuO; Cu/TiO₂; CuO/CNT; Ag; Ag/TiO₂; Ag/CNT and K 30 (Kanamycin disc 30 mcg/ disc).

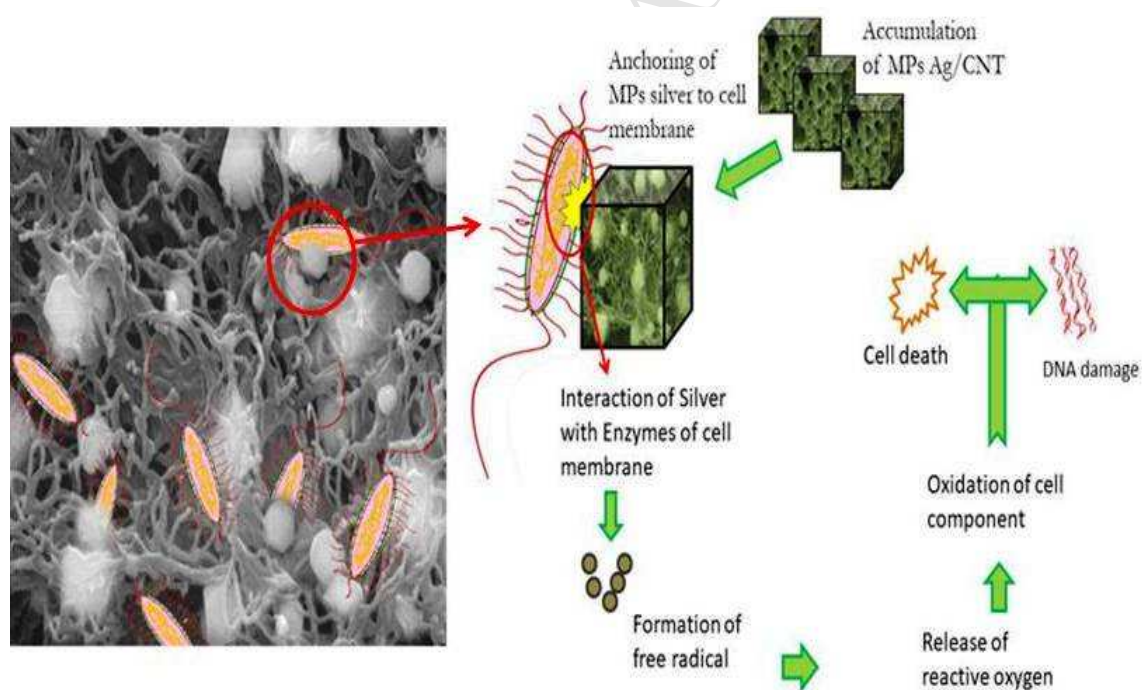


Fig. 9 Systematic mechanisms for bactericidal effects of macroporous Ag/CNT material.

Highlights:

- An efficient, green, acid free, reliable synthetic approach has been explored for the synthesis of macroporous silver and copper oxides monoliths.
- A comparative account of electrochemical sensing property and antimicrobial applications of synthesized monoliths has been developed.
- Efficacious nonenzymatic simultaneous determination of levodopa and ascorbic acid on Ag/TiO₂ and CuO/TiO₂ monoliths modified electrodes shows selective recognition, sensitive and precise determination with low detection limit.
- The synthesized monoliths have also been tested for antimicrobial susceptibility against the eight gram-positive and gram-negative strains for making better candidate of antimicrobial agents.

Graphical abstract:

The systematic pathway of synthesis of hierarchically macroporous Silver and CuO by sol-gel method showed in graphical abstract. A comparative account of electrochemical sensing and antimicrobial applications has been developed.

